Self-similarity of free vibration decays in cantilever beams

Christian Adams[1,2], Sebastian Oberst[2]

[1] *Graz University of Technology, Institute of Fundamentals and Theory of Electrical Engineering, Graz, Austria,*
Email: christian.adams@tugraz.at

[2] *University of Technology Sydney, Centre for Audio, Acoustics and Vibration, Sydney, Australia,*
Email: Sebastian.Oberst@uts.edu.au

Introduction

Free vibrations decay according to a power law in cantilever beams after impact excitation [1]. Power laws are self-similar – an aspect that has so far been regarded as less important in conventional vibration analyses. But from non-linear dynamics point of view, damping is related to negative Lyapunov exponents and phase space contraction. Lyapunov exponents have a spectrum that is related to the Kaplan-Yorke conjecture, which relates dynamic invariants (Lyapunov exponents) to static invariants – the Kaplan-Yorke dimension (as estimate of the fractal dimension). This in turn can then be related to fractality and power laws. This paper will briefly introduce the notion of self-similarity and will explain how the self-similar property of a free vibration decay can enhance our physical understanding of damping in materials. We propose an extended stress-strain relation that is based on Boltzmann's *Theorie der elastischen Nachwirkung* [4],[1] and investigate how it affects the decay of free vibrations in beams.

Here, we measure free vibrations in a cantilever beam, using laser Doppler vibrometry. The vibrations are decomposed into empirical modes, and analysed using the Hilbert-Huang spectrum [1]. The Hilbert-Huang transform combines an empirical mode decomposition with Hilbert spectral analysis. It is a signal processing technique that can adapt to a given dataset without strict a-priori assumptions. This makes the Hilbert-Huang transform a suitable method for the analysis of non-linear or non-stationary signals. However, mode mixing, computational demands and sensitivity to noise must carefully be managed.

Self-similarity and self-similar damping models

Objects are called self-similar if they exhibit similarity on different scales [2], i.e., the object looks identical to a part of itself. Figure 1 shows the Sierpinski triangle, which is a self-similar object. Note that the triangle is composed of three smaller triangles that look similar to the entire triangle. These three triangles are again composed of three smaller triangles and so forth. The Sierpinski triangle on one scale consists of three copies of itself of the next smaller scale. If we were to obtain the Sierpinski triangle shown in Figure 1 from a smaller copy of it, e.g., that in the bottom left, we would need to double its side lengths. Denoting the number of smaller copies by N and the scaling factor, which gives us the Sierpinski triangle from its smaller copy, by M yields the *fractal* dimension

$$D = \frac{\log N}{\log M}. \tag{1}$$

According to Equation (1), the Sierpinski triangle has dimension $D = 1.585$. D is non-integer, which motivates to call objects like the Sierpinski triangle a fractal [2]. The term *dimension* means in this context a physical property of an object, which can be mathematically described. It must be strictly distinguished from the topological dimensions related to integer values of length or other physical concept of dimension, including time, mass, etc. The dimension is generally not equal to the number of spatial coordinates over which an object extends. However, the topological dimensions of well-known (i.e., non-fractal) geometrical objects is equal to the number of spatial coordinates, e.g., a square extends in two spatial coordinates and has dimension $D = 2$.

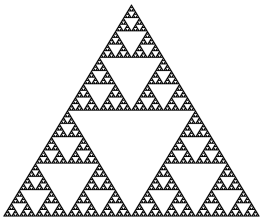

Figure 1: The Sierpinski triangle – an example of a self-similar fractal object

Self-similar damping models are used to model the ultrasonic damping of tissue [6, 7]. These so-called fractal ladder models are rheological topologies of Maxwell elements exhibiting self-similarity, see Figure 2. It is the structure of tissue that motivates the fractal ladder models to account for the damping behaviour on different length scales.

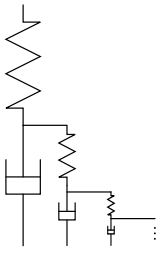

Figure 2: Self-similar ladder model of Maxwell elements

[1] Theory of elastic after effects

The damping of engineering materials such as metals, concrete, or fibre-reinforced plastics is described by one global damping coefficient in many practical applications. The material's topology on different length scales is neglected. Even dependency on frequency is often dropped in practice. This might be acceptable for engineering purposes, but these simplifying assumptions on damping behaviour cannot account for the physical processes involved in the dissipation of vibration energy.

We hypothesise that damping in engineering materials (metals, wood, composites, etc.) exhibit damping effects on different scales. Our hypothesis is motivated by the fact that the topology of these materials is different on length scales: On the macro scale, the material's surface appears smooth but on a lower scale, one finds that the surface shows roughness. Surface roughness is involved in friction effects, which significantly contribute to the damping in assemblies due to micro-motions of jointed surfaces. Fibres of wood or composites are responsible for anisotropic behaviour of such materials, which includes that the wave speed is different for waves travelling parallel or across different fibres. It is likely that also the damping is affected by anisotropy, which lives on the scale of fibre dimensions [3]. Metals, which are isotropic on a macro-scale, become anisotropic on the scale of crystals. Thermal currents along grain boundaries dissipate mechanical energy, which take place on crystal scale [3]. On even smaller scales, the lattice structure contributes to dissipation due to point defects and dislocations [3]. Finally, we reach the atomic scale, where atoms transform vibration energy.

Theory

Boltzmann poses the relation between stress σ and strain ε as follows [4, 5]:

$$\sigma(t) = E_0\varepsilon(t) - \int_0^\infty \varepsilon(t-\Delta t)\Psi(\Delta t)\mathrm{d}(\Delta t), \qquad (2)$$

i.e., stress at time t depends on strain at time t and a constant E_0. Additionally, previous strains at times $(t-\Delta t)$ contribute to the current stress, but to a lesser extent the longer ago this strain occurred. These so-called after-effects are given by the relaxation function

$$\Psi(\Delta t) = \sum_{i=1}^{N} \frac{E_i}{\tau_i} \mathrm{e}^{-\Delta t/\tau_i}, \qquad (3)$$

where N super-imposable relaxation functions with individual relaxation times τ_i are assumed to govern relaxation processes [1]. Assuming harmonic excitation yields the well-known complex modulus

$$E = E^{'} + \mathrm{j}E^{''} = E^{'}(1+\mathrm{j}\eta), \qquad (4)$$

where

$$\eta = \frac{E^{''}}{E^{'}} = \sum_{i=1}^{N} \eta_i \qquad (5)$$

denotes the loss factor [1], and

$$\eta_i = \frac{E_i \frac{\omega\tau_i}{1+\omega^2\tau_i^2}}{E_0 - \sum_{\xi=1}^{N} \frac{E_\xi}{1+\omega^2\tau_\xi^2}}. \qquad (6)$$

Experimental setup

The test setup is illustrated in Figure 3. We measure the time-decaying vibrations at the tip of a cantilever steel beam (length $l = 145\,\mathrm{mm}$, width $b = 16\,\mathrm{mm}$, thickness $h = 1.5\,\mathrm{mm}$,) using laser Doppler vibrometry (Polytec PSV-500 Xtra, Waldbronn, Germany), sampling rate $f_\mathrm{S} = 16\,\mathrm{kHz}$, measurement time 3.1 s, 5 averages, 100 mm/s sensitivity [1].

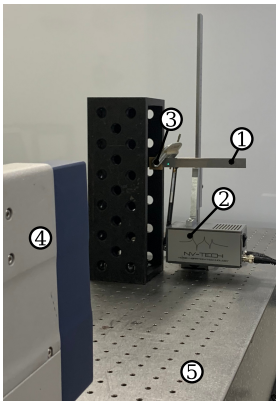

Figure 3: experimental setup, 1: cantilever beam, 2: automatic impact hammer, 3: clamping, 4: laser Doppler vibrometer, 5: vibration-isolated table, [1]

Method

The Hilbert Huang transform decomposes the vibration response $x(t)$ into N variational modes $x_{\mathrm{vm},i}$ according to [8]

$$x(t) = \sum_{i=1}^{N} x_{\mathrm{vm},i} = \sum_{i=1}^{N} A_i(t)\mathrm{e}^{\mathrm{j}\phi_i(t)}, \qquad (7)$$

where $A_i(t)$ and $\phi_i(t)$ are envelope and instantaneous phase of the analytic signal [9]

$$x_{\mathrm{vm},i}(t) = A_i(t)\mathrm{e}^{\mathrm{j}\phi_i(t)} = x_{\mathrm{vm},i}(t) + \mathrm{j}\mathcal{H}\left(x_{\mathrm{vm},i}(t)\right). \qquad (8)$$

$\mathcal{H}$ denotes here the Hilbert transform while the time derivative $\dot{\phi}_i(t)$ represents the instantaneous frequency $\omega_i(t)$ [9]. The variational mode decomposition ensures that each mode decays exponentially [8] so that each mode contains one relaxation process. The intrinsic modes $x_{\mathrm{vm},i}(t)$ are calculated from an optimisation process using an augmented Lagrangian, where the number of modes N and the penalty factor α must be iteratively determined [10]. The penalty factor balances the importance of the properties of the analytic signal (slow varying envelope and exponential decay) with respect to the reconstruction of the original signal using the intrinsic modes (the sum of intrinsic modes yields the original signal) [10].

Results

Figure 4 shows an FFT ($0\ldots8000\,\mathrm{Hz}$, $\Delta f = 0.3215\,\mathrm{Hz}$) of the time decaying vibration of the cantilever beam at its tip as gray solid line, and FFTs of six ($N = 6$) intrinsic modes in colour. Each mode matches one resonance peak of the original signal. Mode coupling happens at $> 30\,\mathrm{dB}$ below the peak levels, which is sufficiently low for the purpose of this analysis. Figures 5 and 6 illustrate the modes when $N = 4$ and $N = 8$, respectively.

In the first case, the number of modes is too low (underfitting). Optimisation is not able to separate the modes well, e.g., modes 1 and 2 are coupled at 1000 Hz. In the second case, the number of modes is too high (overfitting). Information that belongs to one mode is contained in several modes, e.g., modes 3 and 4 or modes 5 and 6 appear at approximately 1000 Hz and 2000 Hz, respectively. The penalty factor $\alpha = 2000$ is chosen as sufficient value for the decomposition into intrinsic modes. Lower values will cause underfitting similar to that shown in Figure 5, while much higher values ($\alpha > 8000$) causes overfitting similar to that shown in Figure 6 except that some peaks will miss a corresponding mode, since the number of modes $N = 6$ is kept. $\alpha = 2000$ represents the lowest acceptable value, where modes appear at the peaks of the original signal and coupling to other modes is sufficiently low. Mode energy over time, instantaneous frequency and envelope are obtained from a Hilbert-Huang spectral analysis. The relaxation times are calculated using regression analysis of the envelopes [1]. Table 1 lists the central frequencies, relaxation times, maximum energy levels, and the time when the intrinsic modes reach their energy maximum.

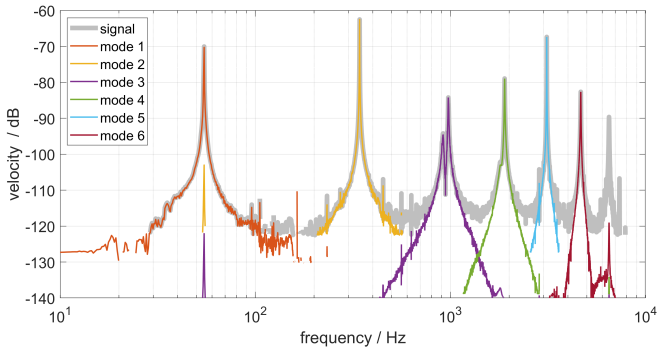

Figure 4: FFT of the vibration decay and intrinsic mode functions, $N = 6$, $\alpha = 2000$

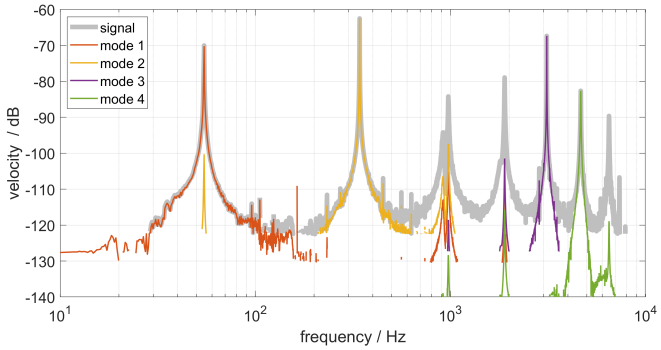

Figure 5: FFT of the vibration decay and intrinsic mode functions, $N = 4$, $\alpha = 2000$

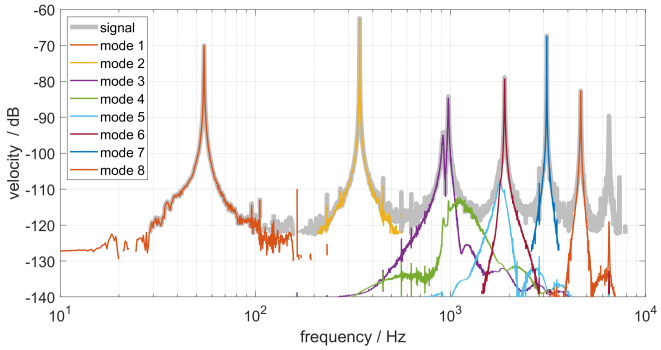

Figure 6: FFT of the vibration decay and intrinsic mode functions, $N = 8$, $\alpha = 2000$

Relaxation times distribute approximately over three orders of magnitude ($10^{-2} \ldots 10^{0}$ s). Although each intrinsic mode decays exponentially, the vibration response itself, i.e., the sum of all intrinsic modes, decays according to a power law. It is the wide range of relaxation times that leads to the power law decay. The power law decay can be estimated from the envelope $A(t)$, which is directly obtained from the Hilbert transform. Regression analysis yields the following equation ($R^2 > 0.99$):

$$A(t) = 1.3 \cdot 10^{-3} \cdot t^{-0.8282}. \tag{9}$$

Power laws are self-similar, i.e., they are scale-free [2]. The exponent of t is non-integer, which suggests that the envelope exhibits fractal properties. The goodness of the power law fit is also validated through visual inspection of the plots in time domain. The high frequency modes with short relaxation times lead to a steep decrease in vibration energy at the early decay. The low frequency modes with longer relaxation times keep vibration energy longer so that the overall vibration decay exhibits a long tail. The self-similar property indicates that relaxation over several times scales leads to the decay of vibration energy [1].

Figure 7 shows the energy of each intrinsic mode over time. Maximum energy levels are marked by a diamond symbol. The values of the diamond location are given in Table 1. It can be seen that the low-frequency intrinsic modes (modes 1 and 2), take longer until they reach their maximum energy level. The other modes reach their maximum energy levels earlier. The maxima of modes 3 to 6 are at similar levels around $-44 \ldots -38$ dB, while modes 1 and 2 take muss less energy. But the energy in modes 1 and 2 persists longer than in modes 3 to 6, which can be seen from the relaxation times (cf. Table 1) and from the energy progression over time in Figure 7.

The instantaneous frequency of the intrinsic modes is illustrated in Figure 8 over time. It can be seen that the instantaneous frequency slightly drops at the beginning, but then remains at the central values (cf. Table 1). Some frequencies tend to slightly oscillate around the central value. These oscillations increase at later times, but most of these oscillations, particularly those of the modes 4 to 6, appear when the modes' energy has decreased below the noise floor so that they are not shown in Figure 8.

Conclusion

It is shown that the free vibrations of a cantilever beam decay by a power law that exhibits fractal and self-similar properties. An estimate of the power law can be obtained from a regression analysis of the vibration response envelope.

Table 1: central frequencies, relaxation times, and energy levels of the intrinsic mode functions

mode number	1	2	3	4	5	6
central frequency / Hz	54.9	342.5	967.4	1895.4	3115.8	4651.9
relaxation time / ms	4380	820	30	40	100	20
maximum energy level / dB	−64	−50	−44	−40	−38	−38
time / ms	31.3	6.8	2.3	2.1	2.7	2.0

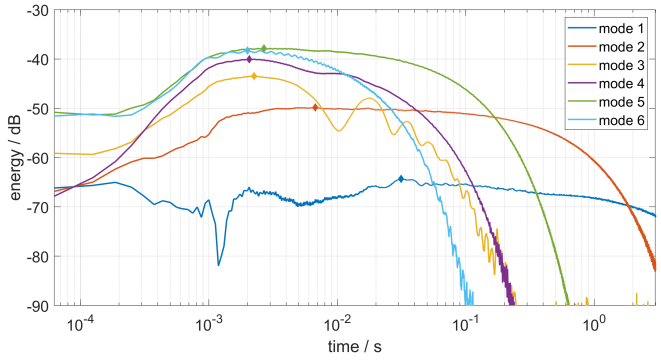

Figure 7: Energy of the intrinsic modes over time, markers are placed at the time, when the energy maximum is reached

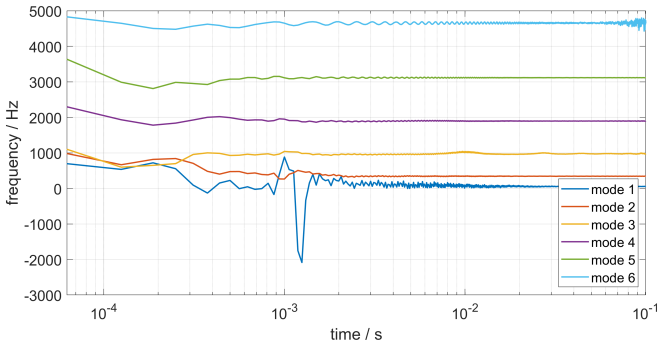

Figure 8: Instantaneous frequency over time of the intrinsic modes

Hilbert-Huang transform is used to decompose the vibration response into several intrinsic modes, each of them decaying exponentially. Exponential decays are enforced in the decomposition using the analytic signal. It is investigated how the number of modes and the penalty factor affect the decomposition. Both parameters need carefully be determined through visual inspection of the FFT-spectra to avoid mode-mixing. If the parameters are set properly, Hilbert-Huang transform adapts itself to the data, which makes the method suitable to study relaxation processes in free vibration decays and capture non-linear and non-stationary signals. However, data quality is essential for a proper decomposition. Slight double hits of the impact hammer or speckles in the vibrometer signal significantly decrease the quality of the Hilbert-Huang transformed signals.

Future work will use the method on different materials to study their relaxation processes. In addition, the relaxation processes should be assigned to the underlying physical processes on the different length scales. We plan to relate our findings to the Lyapunov spectrum, which is illustrated in [11] for a dynamic system. The relation between the Lyapunov spectrum and the fractal dimension is given through the Kaplan-Yorke conjecture [12].

Acknowledgements

CA received from the BMK Endowed Professorship on Noise Impact Research: Competence Center for Traffic Noise and Health of the Austrian Research Promotion Agency (FFG) under project No. FO999891611., SO received funding from the Australian Research Council Linkage funding scheme, project number LP200301196.

References

[1] Adams, C. and Oberst, S.: Multiple energy decay time scales in free vibrating beams and timber rods. Journal of Sound and Vibration (2025), `https://dx.doi.org/10.2139/ssrn.5023548`, under review

[2] Mandelbrot, Benoît B.: The fractal geometry of nature. W. H. Freeman and Co., 1983

[3] Lazan, B. J.: Damping of Materials and Members in Structural Mechanics. Pergamon Press, Oxford, 1968

[4] Boltzmann, L.: Zur Theorie der elastischen Nachwirkung. J. C. Poggendorf Annalen der Physik und Chemie (1878), pp. 624–654, `https://gallica.bnf.fr/ark:/12148/bpt6k15009g?rk=21459;2`

[5] Cremer, L., Heckl, M. and Petersson, B.A.T.: Structure-borne sound: Structural vibrations and sound radiation at audio frequencies. Springer, Berlin, 2005

[6] Szabo, T. L. and Wu, J.: A model for longitudinal and shear wave propagation in viscoelastic media. The Journal of the Acoustical Society of America 107(2000), pp. 2437–2446

[7] Kelly, J. F. and McGough, R. J.: Fractal ladder models and power law wave equations. The Journal of the Acoustical Society of America 126(2009), pp. 2072–2081

[8] Dragomiretskiy, K. and Zosso, D.: Variational mode decomposition. IEEE Transactions on Signal Processing 62(2014), pp. 531–544

[9] Feldman, M.: Hilbert transform in vibration analysis. Mechanical Systems and Signal Processing 25(2011), pp. 735–802

[10] MathWorks, Inc.: Variational mode decomposition Matlab help R2020a. `https://de.mathworks.com/help/wavelet/ref/vmd.html`, accessed: July 31, 2024

[11] Nichols, J.M., Virgin, L.N. and Gavin, H.P.: Damping estimates from experimental non-linear time-series. Journal of Sound and Vibration 246(2001), pp. 815–827

[12] Nichols, J. M., Todd, M. D., Seaver, M., Trickey, S. T., Pecora, L. M. and Moniz, L.: Controlling system dimension: A class of real systems that obey the Kaplan-Yorke conjecture. Proceedings of the National Academy of Sciences 100(2003), pp. 15299–15303